Int. J. Engng Sci. Vol. 24, No. 1, pp. 41–54, 1986
Printed in Great Britain.

0020-7225/86 $3.00 + .00

STEADY STATE PENETRATION OF RIGID PERFECTLY PLASTIC TARGETS

R. C. BATRA
University of Missouri-Rolla, Rolla, MO 65401, U.S.A.

and

T. W. WRIGHT
Ballistic Research Laboratory, Aberdeen Proving Ground, MD 21005, U.S.A.

Abstract—The problem of steady penetration by a semi-infinite, rigid penetrator into an infinite, rigid/perfectly plastic target has been studied. The rod is assumed to be cylindrical, with a hemispherical nose, and the target is assumed to obey the Von-Mises yield criterion with the associated flow rule. Contact between target and penetrator has been assumed to be smooth and frictionless. Results computed and presented graphically include the velocity field in the target, the tangential velocity of target particles on the penetrator nose, normal pressure over the penetrator nose, and the dependence of the axial resisting force on penetrator speed and target strength.

INTRODUCTION

IN SIMPLE THEORIES of penetration the material properties of target and penetrator are often represented only by constant characteristic stresses, as for example in Tate [1, 2]. Although this approach leads to results that are qualitatively correct, it can be difficult to use quantitatively. Some of the problems have to do with actual deformations in target and penetrator including lateral motion, and others are associated with the fact that the plastic flow stress is determined only by the deviatoric components of stress whereas the spherical or pressure component, which may be quite large ahead of the penetrator and contributes significantly to the retardation of the penetrator, is unrelated to flow stress. These and other matters have been discussed recently in some detail by Wright [3]. It would be desirable to account for lateral motion and hydrostatic effects in some simple way, but at present the details are insufficiently known to suggest high quality approximations that might be suitable. In developing an engineering model for penetration and perforation, Ravid and Bodner [4] have attempted to meet this difficulty by assuming simple kinematics for the flow around the penetrator and then adjusting some unknown parameters so as to minimize the plastic dissipation. They characterize this procedure as being "a modification of the upper bound theorem of plasticity to include dynamic effects," but even if such a modified theorem is actually valid, at present there is no way to tell how close such a bound might be.

In this article a detailed numerical solution to an idealized penetration problem is presented in an attempt to shed some light on these matters. The approach taken is as follows. Suppose that the penetrator is in the intermediate stages of penetration so that the active target/penetrator interface is at least one or two penetrator diameters away from either target face, and the remaining penetrator is still much longer than several diameters and is still traveling at a speed close to its striking velocity.

This situation is idealized here in several ways. First, it is assumed that the rod is semi-infinite in length and that the target is infinite with a semi-infinite hole. Furthermore, it is assumed that the rate of penetration and all flow fields are steady as seen from the nose of the penetrator. These approximations are reasonable if the major features of the plastic flow field become constant within a diameter or so of the nose of the penetrator, and will be justified *a posteriori* by the calculation.

Next, it is assumed that no shear stress can be transmitted across the target/penetrator interface. This is justified on the grounds that a thin layer of material at the interface either melts or is severely degraded by adiabatic shear. This assumption, together with the previous one, makes it possible to decompose the problem into two parts in which either a rigid rod penetrates a deformable target or a deformable rod is upset at the bottom of a hole in a rigid target. Of course, in the combined case the contour of the hole is unknown, but if it can be chosen so that normal stresses match in the two cases along the whole boundary between penetrator and target, then the complete solution is known irrespective of the relative motion at the boundary. Even without matching the normal stresses, it would seem that valuable qualitative information about the flow field and distribution of stresses can be gained if the chosen contour is reasonably close to those that are actually observed in experiments.

Finally, the deforming material is assumed to be rigid/perfectly plastic. This assumption should be adequate for examining the flow and stress fields near the penetrator nose, but will lose accuracy with increasing distance, since it forces the effects of compressibility and wave propagation to be ignored.

In this study only the case of the deforming target and a rigid penetrator is considered, where the penetrator is assumed to have a circular cylindrical body and a hemispherical nose.

FORMULATION OF THE PROBLEM

With respect to a set of cylindrical coordinate axes fixed to the center of the hemispherical nose of the rigid cylindrical penetrator, equations governing the deformations of the target are

$$\operatorname{div} \mathbf{v} = 0, \tag{1.1}$$

$$\operatorname{div} \sigma = \rho \dot{\mathbf{v}} \tag{1.2}$$

$$= \rho(\mathbf{v} \cdot \operatorname{grad})\mathbf{v}. \tag{1.3}$$

Here σ is the Cauchy stress tensor, ρ is the mass density of the target material, $\mathbf{v}$ is the velocity of a target particle relative to the penetrator, which has absolute velocity $v_0\mathbf{e}$, $\mathbf{e}$ being a unit vector along the axis and in the direction of motion of the penetrator. The operators grad and div signify the gradient and divergence operators on fields defined in the present configuration. Equation (1.1) expresses the balance of mass and implies that the target undergoes only volume preserving deformations so that the mass density of the target stays constant. Equation (1.2) expresses the balance of linear momentum in the absence of body forces and holds in all Galilean coordinate systems. In particular it holds in one that translates at the constant velocity of the penetrator. Equation (1.3) holds only in such a translating system where all field variables are independent of time. The target material is assumed to obey the Von-Mises yield criterion and the associated flow rule. That is (Prager and Hodge [5]),

$$\sigma = -p\mathbf{1} + \frac{\sigma_0}{\sqrt{3I}}\mathbf{D}, \tag{2.1}$$

$$\mathbf{D} = (\operatorname{grad} \mathbf{v} + (\operatorname{grad} \mathbf{v})^T)/2, \tag{2.2}$$

$$I = \tfrac{1}{2} \operatorname{tr} (\mathbf{D}^2). \tag{2.3}$$

In eqns (2) p is the hydrostatic pressure (which, of course, cannot be determined by the deformation because of the assumption of incompressibility), $\mathbf{1}$ is the identity matrix, $\mathbf{D}$ is the strain rate tensor, σ_0 is the flow stress of the target material in simple compression and tr $(\mathbf{D}^2)$ equals the sum of the diagonal terms of the square matrix $\mathbf{D}^2$. Equation (2.1) is the constitutive relation of an incompressible Navier-Stokes fluid with viscosity coefficient equal to $\sigma_0/2\sqrt{3I}$. Equations (2), when substituted into (1.3), give the field equation

$$-\operatorname{grad} p + \sigma_0 \operatorname{div} ((\operatorname{grad} \mathbf{v} + (\operatorname{grad} \mathbf{v})^T)/2\sqrt{3I}) = \rho(\mathbf{v} \cdot \operatorname{grad})\mathbf{v} \tag{3}$$

which together with (1.1) is to be solved for p and $\mathbf{v}$ subject to suitable boundary conditions. Before stating these, the following nondimensional variables will be introduced:

$$\bar{\sigma} = \sigma/\sigma_0, \qquad \bar{\mathbf{v}} = \mathbf{v}/v_0, \qquad \bar{r} = r/r_0, \qquad \bar{z} = z/r_0, \qquad \bar{p} = p/\sigma_0.$$

The pair (r, z) denotes the cylindrical coordinates of a point with respect to axes attached to the center of the hemispherical nose with the positive z axis pointing into the target material. Rewriting eqns (1.1) and (1.3) in terms of nondimensional variables, dropping the superimposed bars, and agreeing to denote the gradient and divergence operators in nondimensional coordinates by grad and div, we arrive at the following set of equations:

$$\operatorname{div} \mathbf{v} = 0, \tag{4.1}$$

$$-\operatorname{grad} p + \operatorname{div}((\operatorname{grad} \mathbf{v} + (\operatorname{grad} \mathbf{v})^T)/2\sqrt{3I}) = \alpha(\mathbf{v}\cdot\operatorname{grad})\mathbf{v}, \tag{4.2}$$

where $\alpha = \rho v_0^2/\sigma_0$ is a nondimensional number.

Boundary conditions must be given both for the penetrator/target interface and for points remote from the penetrator. As stated in the introduction the interface conditions are

$$\begin{aligned} \mathbf{t}\cdot(\sigma\mathbf{n}) &= 0, \\ \mathbf{v}\cdot\mathbf{n} &= 0, \end{aligned} \tag{5}$$

where $\mathbf{n}$ is a unit normal on the surface and $\mathbf{t}$ is a unit tangent on the surface. At points far away from the penetrator,

$$|\mathbf{v} + v_0\mathbf{e}| \to 0 \quad \text{as} \quad |\mathbf{x}| = (r^2 + z^2)^{1/2} \to \infty, \quad z > -\infty, \tag{6.1}$$

$$|\sigma\mathbf{n}| \to 0 \quad \text{as} \quad z \to -\infty, \tag{6.2}$$

where $\mathbf{e}$ is a unit vector in the positive z direction, as before. The boundary conditions (5) state that the contact surfaces between target and penetrator are smooth and there is no interpenetration of the target material into the penetrator or vice versa. The boundary condition (6.1) is equivalent to the statement that target particles at a large distance from the penetrator appear to be moving at a uniform speed with respect to it. Equation (6.2) states that far to the rear the traction field vanishes. Note that the governing eqns (3) are nonlinear in $\mathbf{v}$ and that a solution of (1.1) and (1.3) under the stated boundary conditions, if there is one, will depend on the rates at which the quantities in (6) tend towards zero.

FINITE ELEMENT FORMULATION OF THE PROBLEM

In order to solve the problem numerically, it is possible to consider only a finite region of the target, and since deformations of the target are axisymmetric, only the target region shown in Fig. 1 is studied. Whether the region considered is adequate or not can be easily decided by solving the problem for two different values of the parameter a. If the two solutions so obtained are essentially equal to each other in the vicinity of the penetrator, then the region studied is sufficient and the effect of boundary conditions at the outer surface EFA has a negligible effect on the deformations of the target material in close proximity to the penetrator. The boundary conditions imposed on the finite region are

$$\sigma_{zz} = 0, \quad v_r = 0 \text{ on the bottom surface AB}, \tag{7.1}$$

$$\mathbf{t}\cdot\sigma\mathbf{n} = 0, \quad \mathbf{v}\cdot\mathbf{n} = 0 \text{ on the common interface BCD}, \tag{7.2}$$

$$\sigma_{rz} = 0, \quad v_r = 0 \text{ on the axis of symmetry DE}, \tag{7.3}$$

$$v_r = 0, \quad v_z = -1.0 \text{ on the boundary surface EFA}. \tag{7.4}$$

A weak formulation of the problem is now obtained. Let $\boldsymbol{\phi}$ be a smooth, vector valued function defined on the region R of the target (shown enclosed by ABCDEFA in Fig. 1), where $\boldsymbol{\phi}$ satisfies the velocity boundary conditions included in eqns (7.1)–(7.3) and $\boldsymbol{\phi} = \mathbf{0}$ on the surface EFA. In addition let ψ be a bounded, scalar valued function defined on R. Taking the inner product of both sides of eqn (4.1) with ψ and of equation (4.2) with $\boldsymbol{\phi}$, integrating the resulting equations over R, using the divergence theorem, the

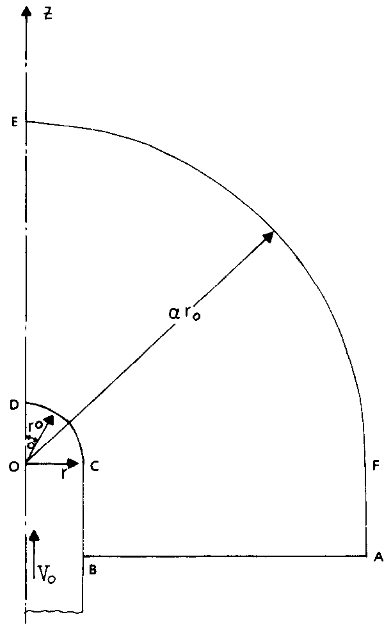

Fig. 1. The region to be studied.

stress boundary conditions in (7) and the stated boundary conditions for ϕ, we arrive at the following equations:

$$\int_R \psi(\operatorname{div} \mathbf{v})\mathrm{d}V = 0, \tag{8.1}$$

$$\int_R p(\operatorname{div} \phi)\mathrm{d}V - \int_R \frac{1}{2\sqrt{3I}} \mathbf{D}\colon (\operatorname{grad} \phi + (\operatorname{grad} \phi)^T)\mathrm{d}V = \alpha \int_R \{(\mathbf{v}\cdot\operatorname{grad})\mathbf{v}\}\cdot\phi\,\mathrm{d}V. \tag{8.2}$$

The boundary value problem defined by eqns (4) and (7) is equivalent to the statement that eqns (8) hold for every ϕ and ψ such that grad ϕ and ψ are square integrable over R, ϕ satisfies the stated homogeneous boundary conditions, and $\mathbf{v}$ satisfies all the velocity boundary conditions stated in (7).

An approximate solution of eqns (8) has been obtained by using the finite element method (see Becker, Carey, and Oden [6] for details). Since eqn (8.2) is nonlinear in $\mathbf{v}$, the following iterative technique has been used:

$$\int_R \psi(\operatorname{div} \mathbf{v}^m)\mathrm{d}V = 0,$$

$$\int_R p^m(\operatorname{div} \phi)\mathrm{d}V - \int_R \frac{1}{2\sqrt{3I^{m-1}}} \mathbf{D}^m\colon (\operatorname{grad} \phi + (\operatorname{grad} \phi)^T)\mathrm{d}V$$

$$= \alpha \int_R \{(\mathbf{v}^{m-1}\cdot\operatorname{grad})\mathbf{v}^m\}\cdot\phi\,\mathrm{d}V, \tag{9}$$

where m is the iteration number. For $\alpha < 2$, the initial solution was taken to be zero everywhere, and for $\alpha \geq 2$, the solution for a smaller value of α was taken as the initial solution. The iterative process was stopped when, at each nodal point,

$$\|\mathbf{v}^m - \mathbf{v}^{m-1}\| \leq 0.01\|\mathbf{v}^{m-1}\|, \tag{10}$$

where the norm is defined by $\|\mathbf{v}\| = (v_r^2 + v_z^2)^{1/2}$. Whereas for problems with $\alpha < 2$, it took nearly 30 iterations for the convergence criterion (10) to be satisfied, problems with $\alpha \geq 2$ required as many as 50 iterations.

COMPUTATION AND DISCUSSION OF RESULTS

A computer code employing six-noded isoparametric triangular elements has been written to solve the problem described above. Both the trial solution ($\mathbf{v}$, p) and the test functions ($\boldsymbol{\phi}$, ψ) are taken to belong to the same space of functions. Whereas, for the triangular element, $\mathbf{v}$ is defined in terms of its values at all six nodal points, the pressure field p is defined only in terms of its values at the corner nodes. The integrations in eqns (9) are performed by using the four-point Gaussian quadrature rule. Since the curved surface of the penetrator nose is not a natural coordinate surface for the cylindrical geometry, it was found to be easiest to enforce the boundary conditions there by using a Lagrange multiplier technique.

The accuracy of the developed code has been established by solving a hypothetical flow problem for an incompressible Navier-Stokes fluid with uniform viscosity. A body force field was calculated so as to satisfy the balance of linear momentum exactly for an assumed, analytically known velocity field, where the assumed velocities had the essential features of those expected in the penetrator problem. Then the code was used to compute the velocity and pressure fields for that body force. As can be seen from the results for this problem given in the Appendix, the computed fields agree very well with those known analytically. An important difference between the test problem and the penetration problem is that in the former the shear viscosity is taken to be constant, whereas in the latter, it depends on the rate of deformation. Since only a simple modification in the computer code is needed to incorporate this feature, it seems reasonable to assume that the computed solution is close to an analytical solution of the problem. Results presented below have been obtained by using the finite element grid shown in Fig. 2.

Figure 3 shows the velocity field in the target material for $\alpha = 4.0$. The velocity fields for other values of α have a similar pattern. In target points that lie to the rear of the center of the penetrator nose, the flow quickly becomes essentially parallel to the axis of the penetrator. Target points that lie ahead of the penetrator nose and within one penetrator diameter from it have a noticeable radial component of velocity. The

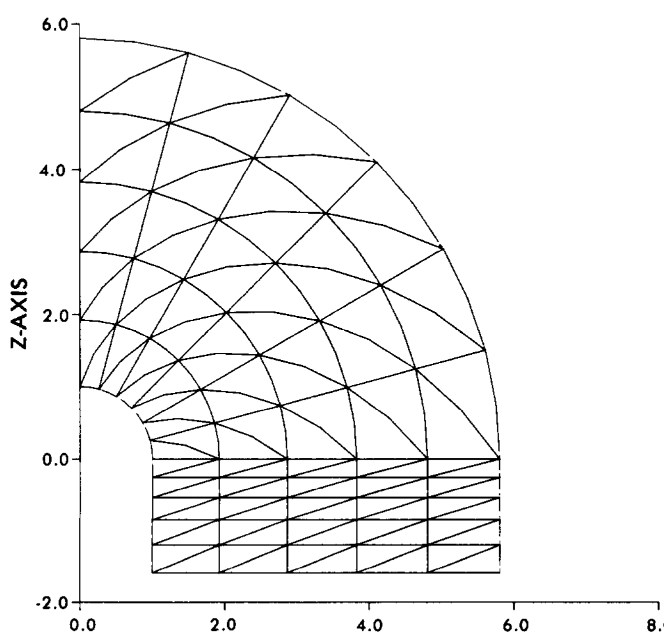

Fig. 2. Finite element grid used.

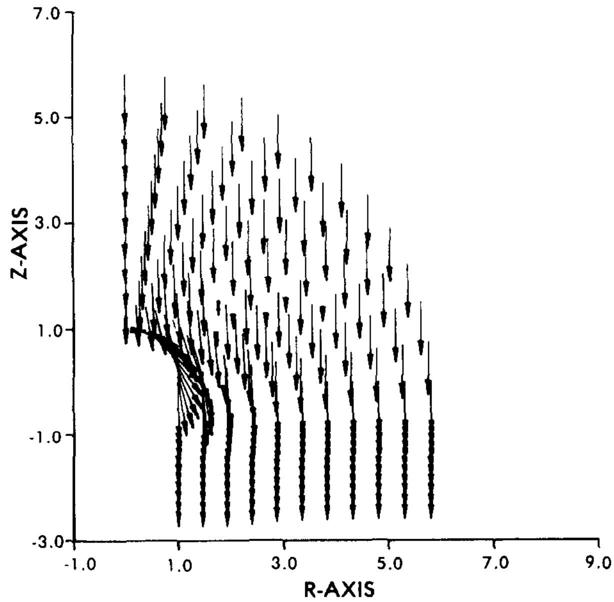

Fig. 3. Velocity field in the target material ($\alpha = 4.0$).

distribution of normal traction on the penetrator nose for various values of α is plotted in Fig. 4. (See Table 1 for identification of the various lines in this and subsequent figures.) Whereas the stress increases with α at the nose tip, it decreases at the sides of the nose. The value of the normal stress for $\theta = 45°$ seems to be independent of α, at least for the range of values of α studied. For $\alpha = 6.15$ the normal stress at approximately $\theta = 83°$ becomes negative, indicating a tendency for the target material to separate from the penetrator nose. Since our formulation of the problem does not allow for separation to occur, we seem to have reached the upper limit for the validity of the calculation, at least for the hemispherical nose shape.

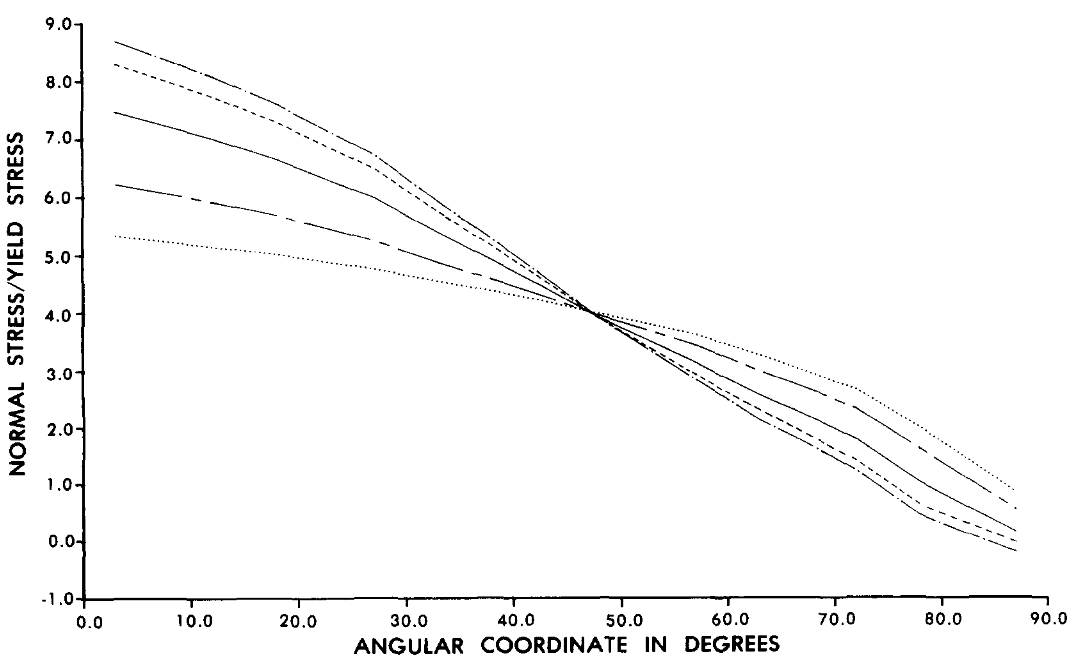

Fig. 4. Normal stress distribution on the hemispherical nose of the penetrator.

Table 1. Legend for figures

Curve Type	α
....	0.72
—— - —— -	2.00
————	4.00
- - - - - - - -	5.43
—— · —— ·	6.15

The total nondimensional force (average stress/flow stress) that acts on the penetrator nose in the negative axial direction is given by

$$F = \int_0^{\pi/2} (\mathbf{n} \cdot \sigma \mathbf{n}) \sin 2\theta \, d\theta.$$

Figure 5, which is a plot of F versus α, shows that F increases only weakly and nearly linearly with α. A close approximation to the line is given by the equation

$$F = 3.903 + 0.0773\alpha, \tag{11}$$

so that in typical impact problems, where the rate of penetration lies roughly in the range $2 \leq \alpha \leq 6$, the retarding force varies only from about 4.1–4.4 times the product of cavity area and compressive flow stress in the target material. Of course this range may change with nose shape, but it does seem to indicate why the choice of constant target resistance in the simple theory of Tate [1, 2] gives such good qualitative results. Note also that, for the same range of α, the centerline stress on the penetrator nose, as shown in Fig. 4, varies from about 5.3–8.8 or as much as twice the average value.

That a significant contribution to the axial force is made by the spherical component of the Cauchy stress σ is clear from Fig. 6, which shows values of nondimensional p in

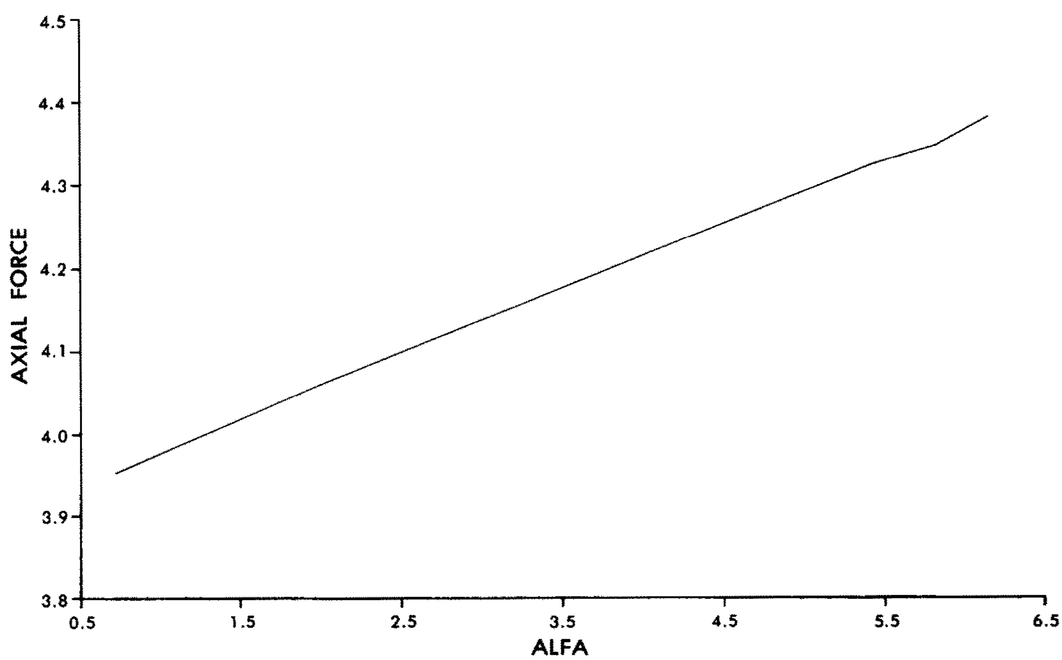

Fig. 5. Axial force vs α.

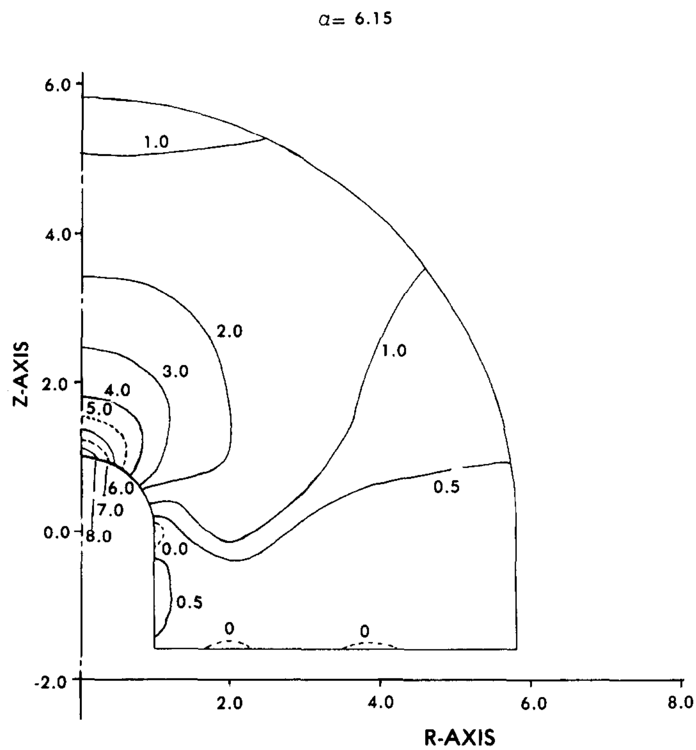

Fig. 6. Contours of p in the target.

the target. Whereas the deviatoric components of σ have magnitudes comparable to the flow stress σ_0, the spherical component p is more than 8 times σ_0 near the nose tip. Figure 7 shows the principal stress components $-\sigma_{zz}$ along the axis in front of the penetrator and demonstrates that stress falls rapidly with distance. The stress near three radii for the smaller values of α cannot be accurately calculated since the velocity gradient there is extremely small.

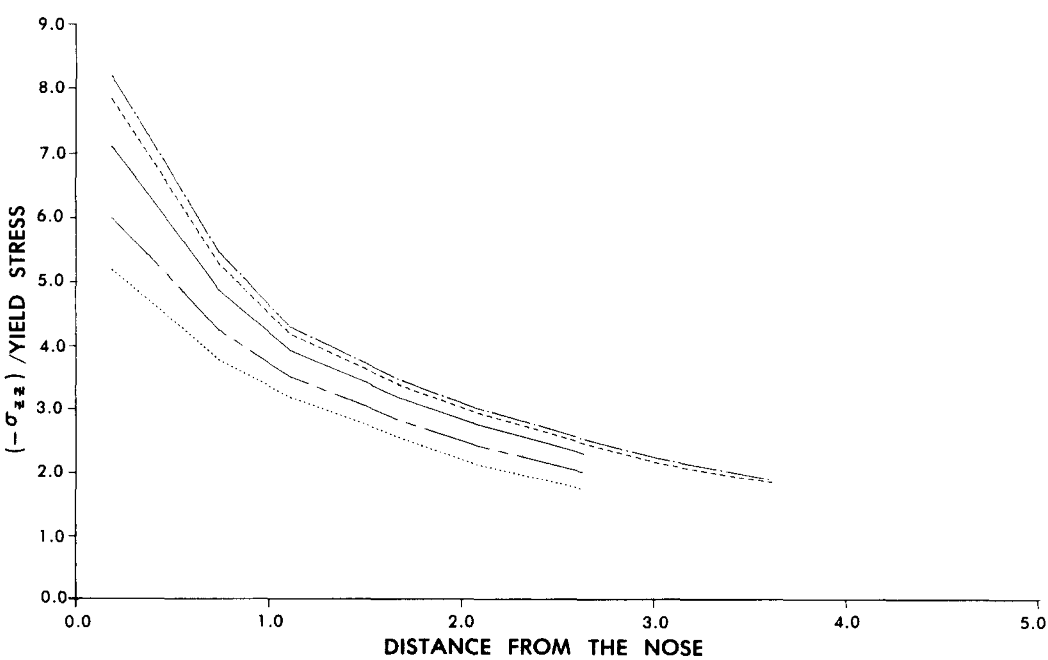

Fig. 7. Variation of $-\sigma_{zz}$ at points of the target along the axis ahead of the penetrator.

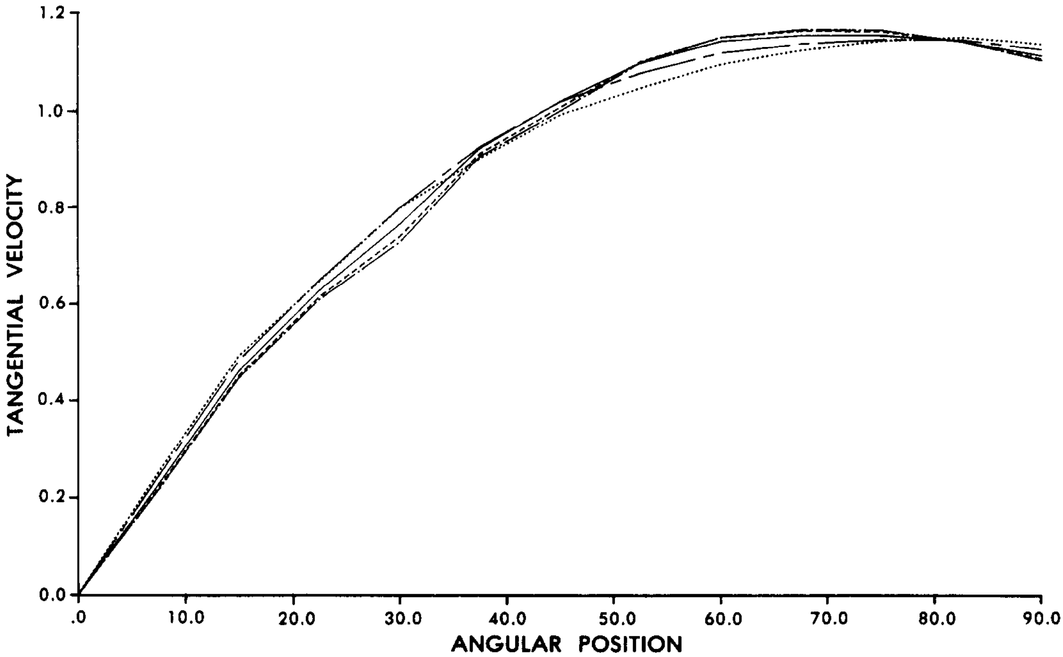

Fig. 8. Tangential velocity distribution on the hemispherical nose of the penetrator.

Figure 8 shows that the nondimensional velocity of target particles, tangential to the penetrator nose, is essentially independent of α, and Fig. 9 shows that the same is true for the axial velocity of target particles along $r = 0$ ahead of the penetrator. Note that the velocity falls more rapidly than stress ahead of the penetrator so that target deformation extends only to about one or two radii away from the nose, whereas the stress is still significant at three radii. The nondimensional values of $\sqrt{I}$, computed for $\alpha = 6.15$, become as large as 2.0 or 2.5 at points close to the nose tip. Since true strain rates scale with v_0/r_0, actual rates in the target may easily be of the order of 10^5 s^{-1} or

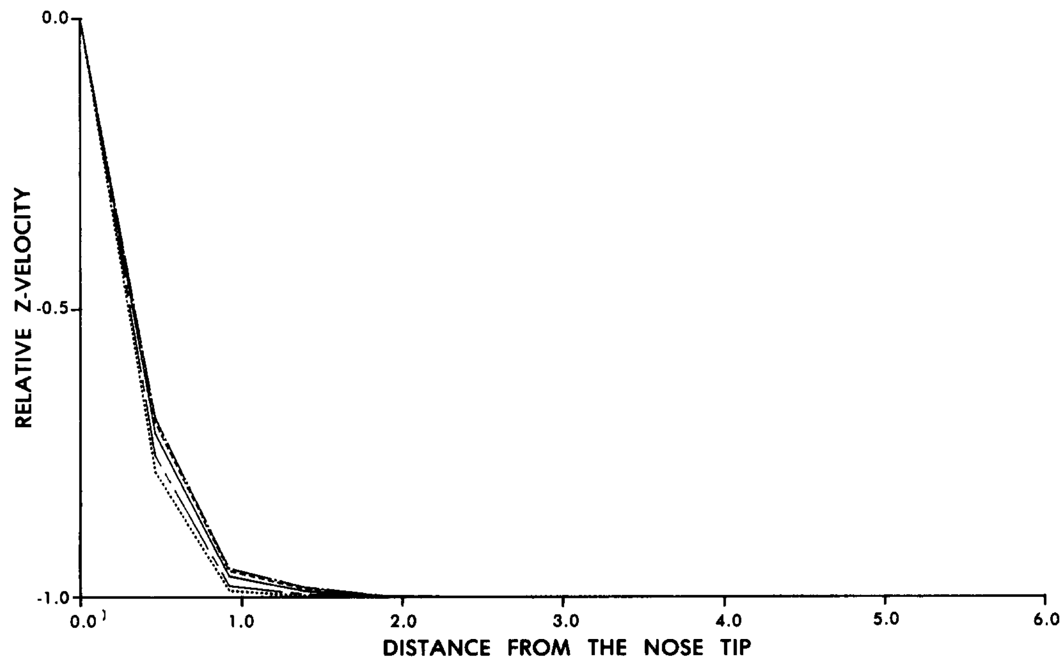

Fig. 9. Variation of the z velocity of target particles along the axis ahead of the penetrator.

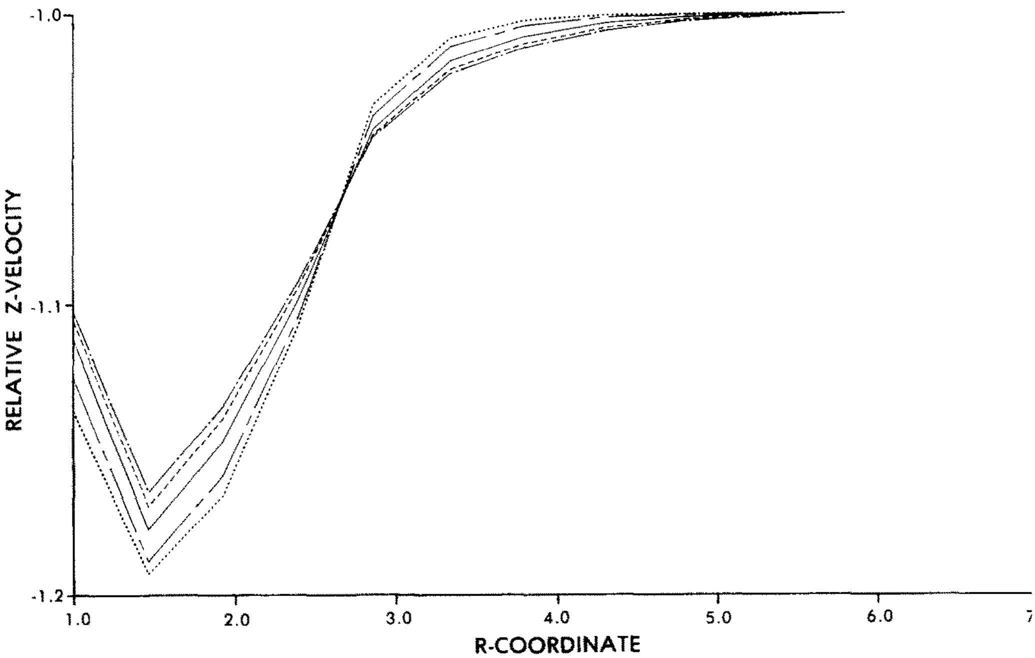

Fig. 10. Variation of v_z with r on the surface $z = 0$.

more for reasonable values of v_0 and r_0. Thus, strain rate effects may become importan in some cases. This should be borne in mind especially for small scale experimenta studies, which will accentuate rate effects and tend to make target materials appea stronger in small scale than in full scale.

Figures 10 and 11 show the variation of v_z with r at $z = 0$ and $z = -1.595$, respectively These results indicate that more of the target material at the sides of the penetrato deforms at higher values of α, even though this is not true ahead of the penetrator a noted in the discussion of Fig. 9. In both Figs. 10 and 11 the nondimensional velocit near the penetrator decreases in absolute value with increasing α in order to satisfy th

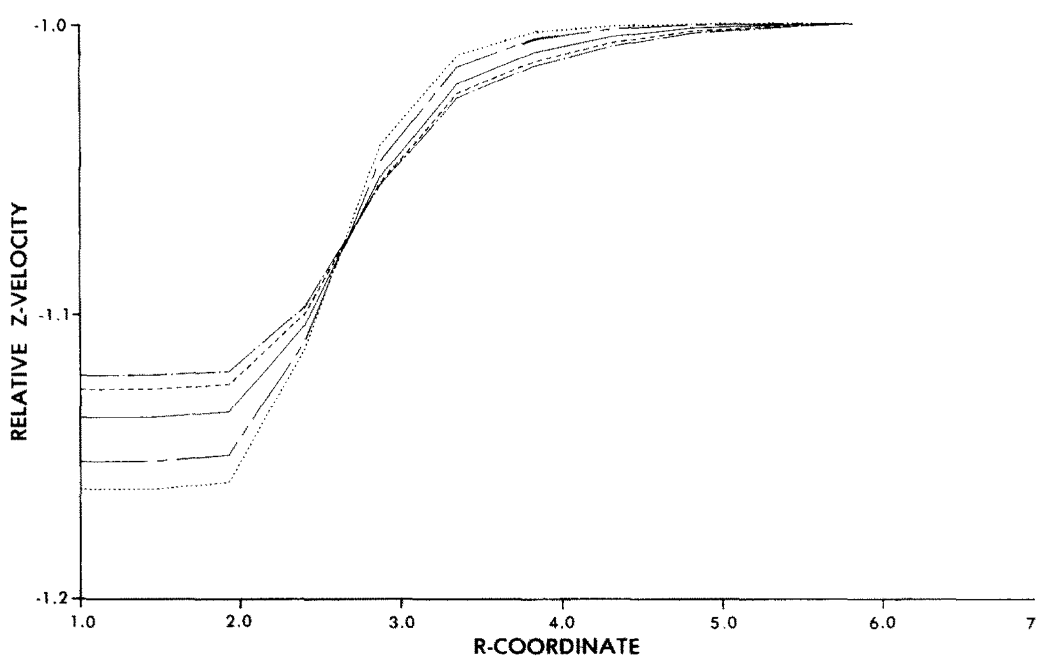

Fig. 11. Variation of v_z with r on the surface $z = -1.595$.

balance of mass. That is to say, since the deformations of the target are volume preserving, the areas between each curve and $v_z = -1.0$ must be constant and just large enough to account for the rate of increase of hole volume as the penetrator advances into the target. Thus the effect of inertia is to spread the deformation farther to the sides, for which compensation must be made closer in so as to maintain incompressibility.

In a recent article, Pidsley [7] described an unsteady calculation for one impact velocity in which both target and penetrator were assumed to be compressible and elastic/perfectly plastic. He shows that, after a few diameters penetration, the rate of penetration slows down and approaches a steady state. Figure 12 compares his values of pressure with the present values of pressure and axial stress along the centerline ahead of the penetrator for nearly the same values of α. Compressibility and thermal expansion apparently have the effect of reducing the pressure directly in front of the penetrator and increasing it at distances greater than one penetrator radius or so, but even so, the results seem to be broadly similar. The fact that the lower pressure contours in Fig. 6 run out to the boundary, rather than closing smoothly as his do, is probably only an artifact due to the proximity of the boundary EFA. It has not been possible to compare velocity fields at all.

In his article Pidsley [7] also notes that if the equation of motion for steady flow is integrated along the central streamline, there is a contribution from transverse gradients of shear stress, unlike the case for a perfect fluid. This fact, which was also noted by Wright [3], may be expressed in the following formula:

$$\tfrac{1}{2}\rho v^2 + p - s_{zz} - 2\int_0^z \frac{\partial \sigma_{rz}}{\partial r}\,\mathrm{d}z = -\sigma_{zz}(0). \tag{12}$$

Each term is evaluated on $r = 0$, s_{zz} is the deviatoric component of stress, and z is measured from the tip of the nose. Figure 13 shows the contributions from the various components in this formula as computed for $\alpha = 5.43$. Since the target material becomes nearly rigid a short distance away from the penetrator nose, the computation of the integrand in (12), which requires differences and divisions with small numbers, is unreliable for $z > 0.6$ or so, so that after that point, the upper bounding line was simply

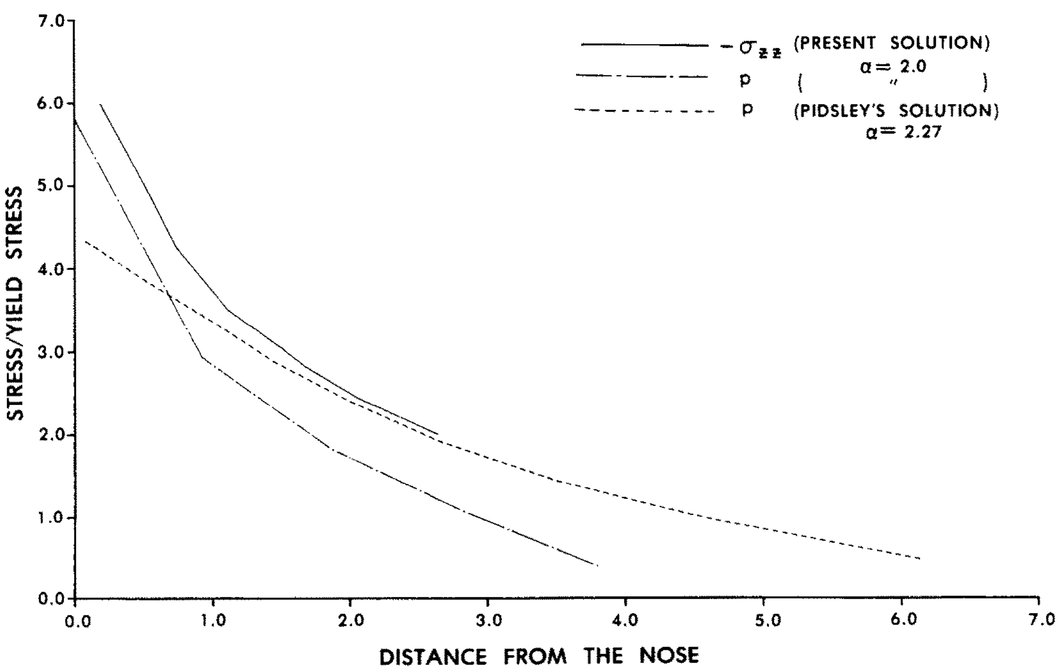

Fig. 12. Comparison of stresses calculated in this paper and in Pidsley [7].

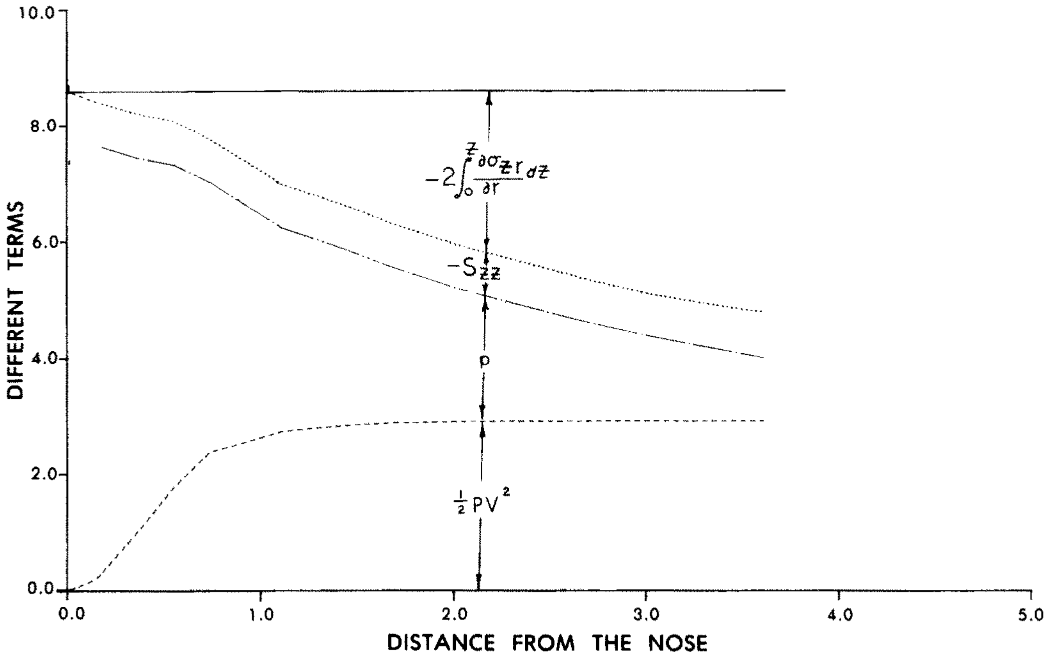

Fig. 13. Contributions to the integral formula (12).

extended horizontally. Note that the integral term in (12) contributes substantially to the total and that the deviatoric component stays nearly constant at approximately 0.75 (compared to the theoretically exact value of $\frac{2}{3}$) out of a total of 8.5.

Since the target deformation is essentially zero at some distance inside the boundary EFA, and since deformations are essentially independent of z near the boundary AB, it seems reasonable to assume that the target region chosen for computations is sufficient to obtain a good description of the deformation in the vicinity of the penetrator nose.

CONCLUSIONS

For the range of values of α studied, noticeable deformation of the target material occurs only at points that are less than three penetrator radii away from the penetrator, and the target seems to deform farther to the side than ahead of the penetrator. The target material adjacent to the sides of the penetrator appears to extrude rearwards in a uniform block that is separated from the bulk of the stationary target by a narrow region with a sharp velocity gradient, but the highest strain rates occur just ahead of the penetrator nose. This calculation of backward extrusion of a uniform block gives at least a partial justification to the velocity field assumed by Ravid and Bodner [4] in their work involving targets of finite thickness. We are not aware of any experimental work that sheds more light on this.

Maximum normal stresses occur at the nose tip, as might be expected, and fall off rapidly away from that point. At the higher values of α, flow separation seems to be indicated at the sides of the nose. The retarding force was found to be a weak linear function of α, and gradients of shear stress were found to make a strong contribution to the momentum integral along the axial streamline.

The kinematics and stress fields found in this study should prove useful in devising or checking the results from simpler engineering theories of penetration.

REFERENCES

[1] A. TATE, *J. Mech. Phys. Solids* **15**, 387 (1967).
[2] A. TATE, *J. Mech. Phys. Solids* **17**, 141 (1969).
[3] T. W. WRIGHT, "A Survey of Penetration Mechanics for Long Rods," in *Lecture Notes in Engineering,*

vol. 3, Computational Aspects of Penetration Mechanics (Edited by J. Chandra and J. Flaherty). Springer-Verlag, New York (1983).
[4] M. RAVID and S. R. BODNER, *Int. J. Engng Sci.* **21**, 577 (1983).
[5] W. PRAGER and P. HODGE, *Theory of Perfectly Plastic Solids.* Dover, New York (1968).
[6] E. BECKER, G. CAREY and J. T. ODEN, *Finite Elements—An Introduction,* Vol. 1. Prentice-Hall, Englewood Cliffs, New Jersey (1981).
[7] P. H. PIDSLEY, *J. Mech. Phys. Solids* **32**, 315 (1984).

(*Received in revised form* 10 *November* 1984)

APPENDIX

We established the validity of the finite element code by solving the following hypothetical problem. Consider the flow of a homogeneous and incompressible Navier-Stokes fluid of unit mass density and unit viscosity. The governing equations are obtained from (1) and (2) by setting $\rho = 1$, $\sigma_0/\sqrt{3}I = 1$ and adding the body force vector **g** to the left-hand side of eqn (1.2). A solution of these equations is

$$v_r = r(1 - r), \qquad v_z = -z(2 - 3r), \qquad p = z, \tag{A1.1}$$

$$g_r = 3 + r(1 - r)(1 - 2r), \tag{A1.2}$$

$$g_z = 1 - 3z/r + 3zr(1 - r) + z(2 - 3r)^2. \tag{A1.3}$$

Here v_r and v_z are, respectively, the radial and axial components of the velocity, and g_r and g_z equal the radial and axial components of the body force per unit mass.

A rather coarse grid, shown in Fig. A1, was used to compute the solution. On surfaces AB, BC and CD, both v_r and v_z as given by eqn (A1.1) were prescribed; on the surface AD, v_r and the normal traction (equal to σ_{zz}) were specified. The computed results obtained after six iterations are compared in Table A1 with the analytical solution at various points of the grid. Recall that the pressure field is computed at nodal points on the corners of an element but can be interpolated at any other point. We note that, whereas computed values of v_r

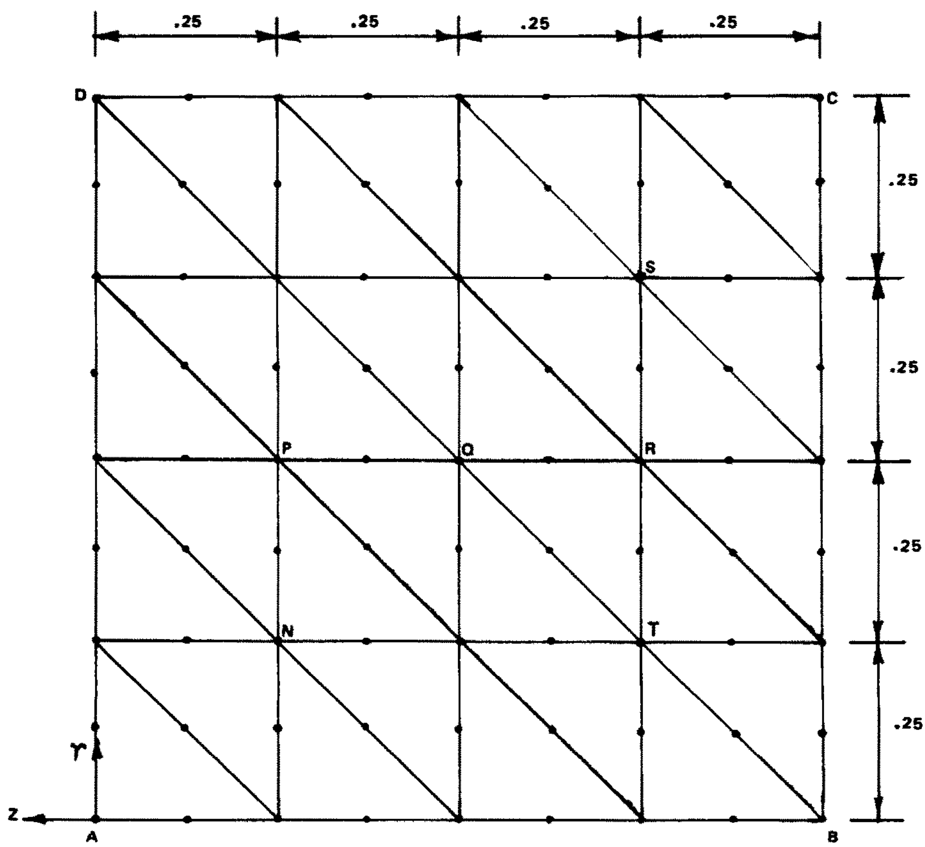

Fig. A1. Grid used to solve the test problem.

Table A1. Comparison of analytical and numerical solution

Point	ANALYTICAL VALUES			COMPUTED VALUES		
	v_r	v_z	$-p$	v_r	v_z	$-p$
N	0.18750	0.31250	0.250	0.18667	0.30954	0.27116
P	0.2500	0.12500	0.250	0.24962	0.12490	0.2510
Q	0.250	0.250	0.500	0.25103	0.249993	0.48991
R	0.250	0.3750	0.750	0.25372	0.37503	0.72261
S	0.18750	-0 18750	0.750	0.18984	-0.18761	0.6804
T	0.18750	0.93750	0.750	0.18966	0.93637	0.8016

and v_z differ at most by one percent from their analytical values, the computed value of p at the point S differs from the analytical value by 9.3%. Of course, the refinement of the grid will result in values of p closer to the analytical values. We believe that the values given in Table A1 do establish the validity of the code.